

A BENCHMARK FOR LABORATORY EXPOSURES WITH 1 A GeV IRON IONS

John W. Wilson¹, John Tweed², Steve A. Walker², Francis A. Cucinotta³, Ram K. Tripathi¹, Steve Blattmig¹,
Christopher J. Mertens¹

¹*NASA Langley Research Center, Hampton VA 23681-2199 USA*

²*Old Dominion University, Norfolk VA 23529 USA*

³*NASA Johnson Space Center, Houston, TX 77058 USA*

ABSTRACT

A new version of the HZETRN code capable of simulating HZE ions with either laboratory or space boundary conditions is under development. The computational model consists of combinations of physical perturbation expansions based on the scales of atomic interaction, multiple scattering, and nuclear reactive processes with use of asymptotic/Neumann expansions with non-perturbative corrections. The code contains energy loss with straggling, nuclear attenuation, nuclear fragmentation with energy dispersion and downshifts, and off-axis dispersion with multiple scattering under preparation. The present benchmark is for a broad directed beam for 1 A GeV iron ion beams with 2 A MeV width and four targets of polyethylene, polymethyl methacrylate, aluminum, and lead of varying thickness from 5 to 30 g/cm². The benchmark quantities will be dose, track averaged LET, dose averaged LET, fraction of iron ion remaining, and fragment energy spectra after 23 g/cm² of polymethyl methacrylate.

INTRODUCTION

Our early interest in transport code development paralleled the experimental studies of Walter Schimmerling et al. (1986) at the Lawrence Berkeley Laboratory and involved solving the Boltzmann transport equation for mono-energetic ion beams in the context of the continuous slowing down approximation (Wilson et al. 1984). The main computational limitation was found to be the inadequacy of available nuclear data by comparing computational results to the ionization data for a broad beam of ²⁰Ne ions (Wilson et al. 1984, Shavers et al. 1993). Emphasis was soon overtaken by the need to establish the scope of the GCR protection problem and marching procedures were used to get first order estimates of shielding requirements (Wilson et al. 1991). Testing the new marching computational model against atmospheric air shower data again pointed to the inadequacy of the available nuclear data (Wilson and Badavi 1986) and development of a semi-empirical nuclear model followed, leading to reduced computational errors (Wilson et al. 1987a, 1987b). The next several years emphasized spaceflight validation of the marching solution and nuclear model improvements (Shinn et al. 1998, Cucinotta et al. 1998, Wilson et al. 1995). Advanced solution methods of the Boltzmann equation continued to develop (Wilson et al. 1994a,b) but only slowly after NASA support for deterministic transport code and nuclear model development ended in 1995 in favor of Monte Carlo methods (Armstrong and Colburn 2001, Pinsky et al. 2001). Recent renewed interest within NASA for deterministic code development is giving new emphasis to improved solution methods, but without the aid of nuclear modeling activity (Wilson et al. 2003). As a result, current developments utilize the older semi-empirical NUCFRG2 model (Wilson et al. 1995b) with energy downshifts and momentum dispersion (Tripathi et al. 1994). Comparison of NUCFRG2 with other models and experiments are given by Zeitlin et al.

(1997). In the current report, we will first review the current status of code development with emphasis on future needs. Within current limitations, we will present the benchmark results requested by the invitation using a newly developed code based on three-term Neumann expansions with nonperturbative corrections above the third Neumann term (Tweed et al. 2004).

DETERMINISTIC CODE DEVELOPMENT

The relevant transport equations are the linear Boltzmann equations derived on the basis of conservation principles (Wilson et al. 1991) for the flux density $\phi_j(\mathbf{x}, \Omega, E)$ for particle type j as

$$\Omega \cdot \nabla \phi_j(\mathbf{x}, \Omega, E) = \sum_k \int \phi_k(\mathbf{x}, \Omega', E') \Sigma_{k \rightarrow j}(\mathbf{x}, \Omega, E, E') d\Omega' dE' - \phi_j(\mathbf{x}, \Omega, E) \Sigma_j(\mathbf{x}, \Omega, E) \quad (1)$$

where $\Sigma_j(E)$ and $\Sigma_{jk}(\mathbf{x}, \Omega, E, E')$ are the shield media macroscopic cross sections. The $\Sigma_{jk}(\mathbf{x}, \Omega, E, E')$ represent all those processes by which type k particles moving in direction Ω' with energy E' produce a type j particle in direction Ω with energy E (including decay processes). Note that there may be several reactions that produce a particular product, and the appropriate cross sections for equation (1) are the inclusive ones. Exclusive processes are functions of the particle fields and may be included once the particle fields are known. The total cross section $\Sigma_j(E)$ with the medium for each particle type is

$$\Sigma_j(E) = \Sigma_{j,at}(E) + \Sigma_{j,el}(E) + \Sigma_{j,r}(E) \quad (2)$$

where the first term refers to collision with atomic electrons, the second term is for elastic scattering on the nucleus, and the third term describes nuclear reactions where we have ignored the minor nuclear inelastic processes. The corresponding differential cross sections are similarly ordered. Many atomic collisions ($\sim 10^6$) occur in a centimeter of ordinary matter, whereas $\sim 10^3$ nuclear coulomb elastic collisions occur per centimeter, while nuclear reactions are separated by a fraction to many centimeters depending on energy and particle type. Solution methods first use perturbations based on the ordering of the cross sections with atomic interactions as the first physical perturbation with special methods used for neutrons for which atomic cross-sections are zero.

We rewrite equation (1) in operator notation by defining a vector array field function as

$$\Phi = [\phi_j(\mathbf{x}, \Omega, E)] \quad (3)$$

the drift operator

$$\mathbf{D} = [\Omega \cdot \nabla] \quad (4)$$

and the interaction operator

$$\mathbf{I} = [\sum_k \int \phi_k(\mathbf{x}, \Omega', E') \Sigma_{k \rightarrow j}(\mathbf{x}, \Omega, E, E') d\Omega' dE' - \phi_j(\mathbf{x}, \Omega, E) \Sigma_j(\mathbf{x}, \Omega, E)] \quad (5)$$

with the understanding that \mathbf{I} has three parts associated with atomic, elastic, and reactive processes as given in equation (2). Equation (1) is then rewritten as

$$[\mathbf{D} - \mathbf{I}_{at} - \mathbf{I}_{el}] \Phi = \mathbf{I}_r \Phi \quad (6)$$

where the first two physical perturbation terms are shown on the left-hand side and are represented by a diagonal operators. The first order physical perturbation

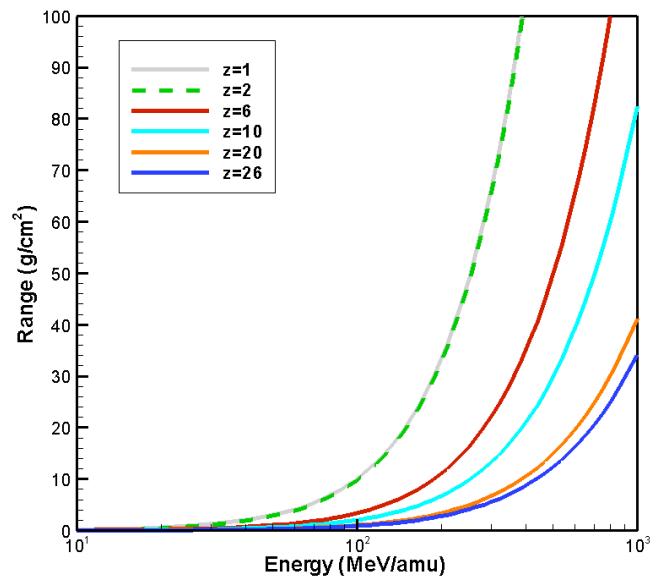


Fig. 1 Range of ions in aluminum.

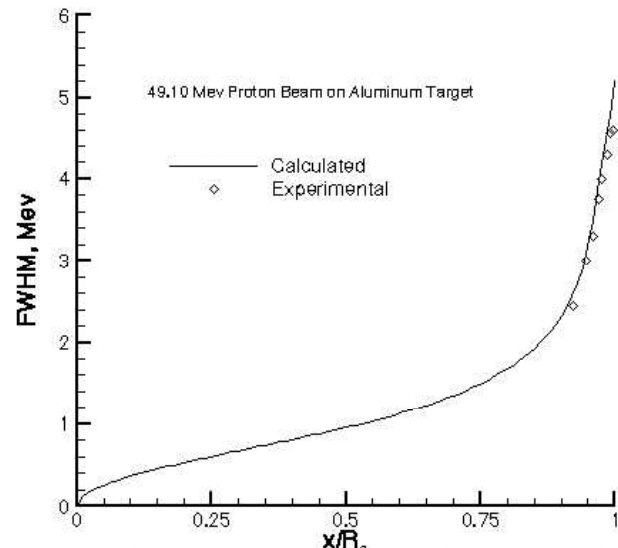


Fig. 2 FWHM of 49.1 MeV protons.

for atomic processes is solution of

$$[D - I_{at}]_{\infty} = 0 \quad (7)$$

using the moments methods and approximated by

$$(z, E) = \exp[-(E - \langle E(z) \rangle)^2 / (2s^2(z))] / (2(\pi)s(z)) \quad (8)$$

where the array of mean residual energies $\langle E(z) \rangle$ and the energy deviation $s(z)$ are evaluated using a second order Green's function (Wilson et al. 2002) and related to range and full width at half maximum (FWHM) shown in Figs. 1 and 2. Although straggling correction for the uncollided beam is important, it is negligible in the higher order terms compared to the energy dispersion in fragmentation.

The second physical perturbation term is the coulomb scattering by the atomic nucleus as a solution of

$$[D - I_{el}]_{\infty} = 0 \quad (9)$$

and represented by Rutherford scattering modified by screening of the nuclear charge by the orbital electrons using the Thomas-Fermi distribution for the atomic orbitals. We will utilize the multiple scattering solutions of Fermi given by

$$(z, r, \theta_r) = [3 w^2 / (2 z^2) \exp[-w^2(\theta_r^2 / z - 3r) / (z^2 + 3r^2 / z^3)]] \quad (10)$$

where z is the longitudinal distance, r is the lateral distance, θ_r is the angle to the longitudinal axis, and w^2 the array of appropriate diffusion coefficients. Strictly speaking, the solution applies only over intervals for which the variation in ion energy is small. It follows that the mean square angle (understood as a differential quantity) in traveling a distance dz is given from equation (10) as

$$\theta_r^2 = 2 dz / w^2 \quad (11)$$

Conversely, one finds for a uniform nuclear charge distribution shielded by a Thomas-Fermi atomic structure

$$\theta_r^2 = dz (Z_p E_s / -pc)^2 / X_0 \quad (12)$$

so that

$$w^2 = 2X_0 (-pc Z_p)^2 \quad (13)$$

where

$$E_s = (4(\alpha^2 / c)) = 21.2 \text{ MeV} \quad (14)$$

with α the fine structure constant, p the ion momentum array, the array $-$ of ion speeds relative to the speed of light c , Z_p the array of projectile charges, and X_0 is the electron radiation length in the material. The electron radiation length (g/cm^2) is given by

$$X_0^{-1} = 4 (N_A / A) Z_T^2 r_0^2 \ln(181 Z_T^{-1/3}) \quad (15)$$

with Avagadro's number N_A , A the molecular weight, and r_0 the classical electron radius. We will be using Schimmerling and coworkers modifications to Fermi's width formula (1986, Wong et al. 1989). Multiple scattering played a critical role in prior experimental validation of the transport solutions (Shavers et al. 1990, 1993). An example of multiple Coulomb scattering is given in Fig. 3 showing the emerging ion angular distribution on the beam axis and off the beam axis for 600 A MeV iron ions in aluminum. The iron ions on the beam axis remain highly peaked in the forward direction while those that have scattered off axis exhibit wider angular divergence. In all cases the angular dispersion is small and clearly will be important only for the uncollided beam ions.

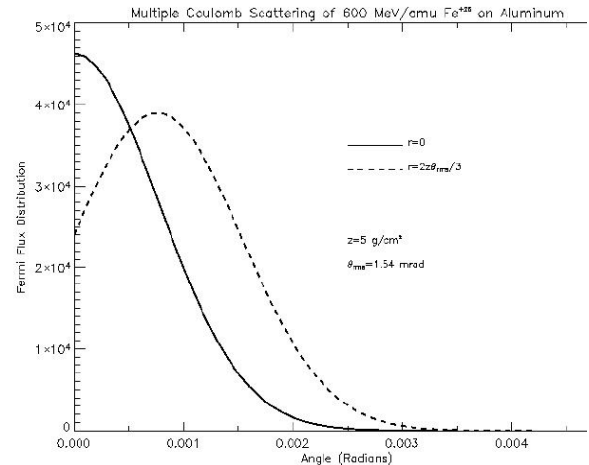


Fig. 3 Multiple Coulomb scattering of 600 A MeV iron ions in a 5 g/cm^2 aluminum target.

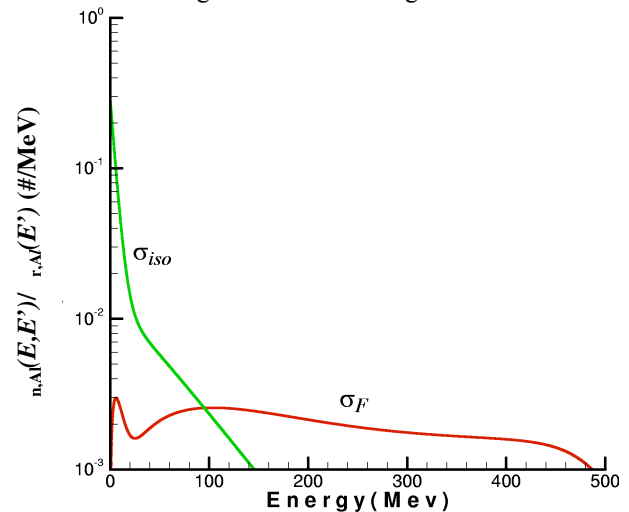


Fig. 4 Isotropic and forward neutron spectra produced by 500 MeV proton in aluminum.

The third order physical perturbation involves the nuclear reactive processes represented by the operator I_r of equation (6), rewritten as follows

$$[D - I_{at} - I_{el} + I_r]^\infty = \left\{ \int_r(\theta, E, E') d\theta' dE' \right\}^\infty \quad (16)$$

The off-diagonal nuclear reactive differential cross sections can be written in the following form

$$g_{jk,r}(\theta, E, E) = g_{jk,iso}(E, E)/4 + g_{jk,for}(\theta, E, E) \quad (17)$$

where the first term is isotropic and associated with lower energy particles produced including target fragments and the second term is highly peaked in the forward direction and is associated mainly with direct quasi-elastic events and projectile fragmentation products (Wilson 1977, Wilson et al. 1988). Surprisingly, even nucleon-induced reactions follow this simple form and the isotropic term extends to relatively high energies (see Fig. 4). For nucleon induced reactions, the following form has been used in versions of FLUKA (Ranft 1980) as follows

$$g_{jk,r}(\theta, E, E) = 2_{jk}(E) g_{jk,r}(E) f_{jk}(E, E) \quad (18)$$

where $2_{jk}(E)$ is multiplicity and the Ranft factor used in FLUKA is

$$g_{jk,r}(\theta, E, E) = N_R \exp[-\theta^2 / R] (2) \quad (19)$$

and constant for larger values of production angle θ , N_R is normalization constant, and R given by Ranft as

$$R = (0.12 + 0.00036 A_T / E) \quad (20)$$

although new generalized fits are being derived. This separation in phase space will be further exploited in computational procedures. The heavy ion projectile fragment cross sections are further represented by

$$g_{jk,for}(\theta, E, E) = g_{jk,r}(E) N_t \exp[-2m(E)(1 - \cos\theta) / t_{jk}] \exp[-(E + g_{jk} - E)^2 / 2 g_{jk}^2] / (2 g_{jk}^2) \quad (21)$$

where g_{jk} is related to the momentum downshift, t_{jk} is related to the longitudinal momentum width, g_{jk} is related to the transverse momentum width, and N_t is the transverse normalizing factor. Since the transverse width is small compared to the projectile and fragment energy the transverse function is highly peaked about the forward direction ($\theta \approx 0$).

Atomic interactions limit the contributions of charged particles in the transport process. For example, the protons and alpha particles produced in aluminum below 100 A MeV contribute to the fluence only within a few centimeters of their collision source and the heavier ions are even more restricted (see Fig. 1). This is an important factor in that the transported secondary charged particle flux tends to be small at low energies and the role of additional nuclear reactions are likewise limited (see Fig. 5).

The reaction cross section is separated by equation (17) into isotropic and forward component for which equation (16) may be written as coupled equations

$$[D - I_{at} - I_{el} + I_r]^\infty_{for} = \left\{ \int_r(\theta, E, E') d\theta' dE' \right\}^\infty_{for} \quad (22)$$

and

$$[D - I_{at} - I_{el} + I_r]^\infty_{iso} = \left\{ \int_r(\theta, E, E') d\theta' dE' \right\}^\infty_{iso} + \left\{ \int_r(\theta, E, E') d\theta' dE' \right\}^\infty_{for} \quad (23)$$

Equation (22) can be written as a Volterra equation (Wilson 1977, Wilson et al. 1991) and solved as

$$I_{for} = [G + G \odot I_{for} \odot G + G \odot I_{for} \odot G \odot I_{for} \odot G + \dots] \odot B \quad (24)$$

for which the series can be evaluated directly as described elsewhere (Wilson et al. 1994a).

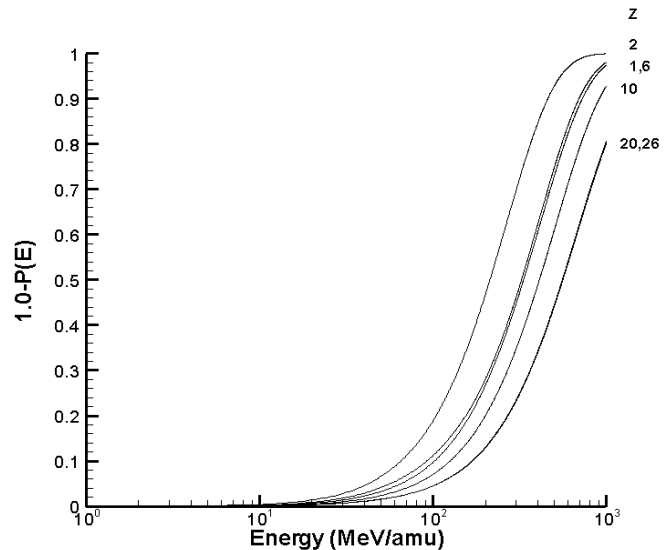


Fig. 5 Probability of nuclear reaction as a function of ion type and energy.

The cross term in equation (23) gives rise to a nearly isotropic source of light ions of only modest energies and neutrons. The high-energy portion of the isotropic spectra arises from multiple scattering effects and the Fermi motion of the struck nucleons within the nucleus. The low-energy isotropic spectra arise from decay processes of the struck nucleus. Spectral contributions to the Neumann series depend on the particle range and probability of surviving nuclear reactions that establish the functional form of the \mathbf{G} matrix. The second term of the Neumann series is proportional to the probability of nuclear reaction that is limited by the particle range as discussed above and shown in Fig. 5. It is clear from Fig. 5 that those nuclear reactions for the charged particles below a few hundred A MeV are infrequent for which fast convergence of the Neumann series is expected. For the moment we will neglect the straggling and multiple-elastic processes to simplify the present explanation (these provide only minor corrections to space radiation exposures but important in laboratory testing) and examine the remaining reactive terms of equation (22). The corresponding Volterra equation is given (Wilson 1977) by

$$j(\mathbf{x}, E) = \{S_j(E)P_j(E) \int_{k_o} j(\mathbf{x}', E) + \int_E^E dE' A_j P_j(E') \int_{k_o} d\Omega' j_{k,for}(\mathbf{x}', E', E) \} / S_j(E)P_j(E) \quad (25)$$

where \mathbf{x}' is the point on the boundary connected to \mathbf{x} along \mathbf{s} , $E' = E - d + R_j$, \mathbf{s} is the projection of \mathbf{x} onto the boundary, and d is the projection of \mathbf{x} onto the boundary. Equation (24) results from the Neumann series solution to equation (25). In the past we have expanded the angular integral over Ω' asymptotically and implemented as a marching procedure (HZETRN, Wilson and Badavi 1986), as a perturbation expansion (Wilson et al. 1984), and by non-perturbative approximation (Wilson et al. 1994a) resulting in three distinct methods to evaluate the first order asymptotic terms, all of which have had extensive experimental validation (Shavers et al. 1993, Wilson et al. 1998, Shinn et al. 1998). Independent of the method used to evaluate the lowest order term, the first correction term is found by replacing the fluence in the integrand of equation (25) by the lowest order asymptotic solution as

$$j(\mathbf{x}, E) = \{S_j(E)P_j(E) \int_{k_o} j(\mathbf{x}', E) + \int_E^E dE' A_j P_j(E') \int_{k_o} d\Omega' j_{k,for}(\mathbf{x}', E', E) \} / S_j(E)P_j(E) \quad (26)$$

where $j(\mathbf{x}, E)$ is found as an integral over the neighborhood of rays centered on \mathbf{x} using the lowest order asymptotic solution $j_{k,o}(\mathbf{x}, E)$ along an adjacent ray directed along \mathbf{s} . Note that the boundary condition reached along \mathbf{s} enters through the lowest order asymptotic approximation and the angular integral correction in equation (25) is determined by the homogeneity and angular dependence of the space radiation and radius of curvature of the bounding material as we have shown long ago (Wilson and Khandelwal 1974, Wilson 1977). These are the determinant factors of the magnitude of the first order asymptotic correction which is anticipated to be very small for human rated systems (large radius of curvature) in space radiation which is homogeneous and isotropic in most applications (Wilson et al. 1991, Wilson et al. 1994b).

In a region of small radius of curvature the specific flux components near the site of evaluation will be missing contributions along adjacent rays which do not compensate losses along the ray on which the solution is evaluated representing the losses due to leakage. (Note, an asymptotic treatment of such small angle dependent phenomena is the only useful approach circumventing large discretization errors.) This computational procedure is only a small addition to prior code development and will have little impact on computational efficiency. The angular dependence of the

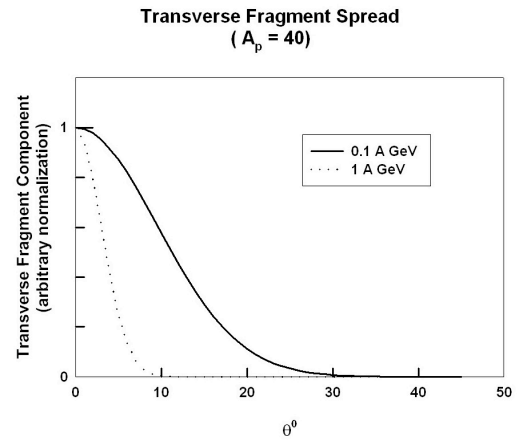


Fig. 6 Normalized transverse components for Ca fragmentation.

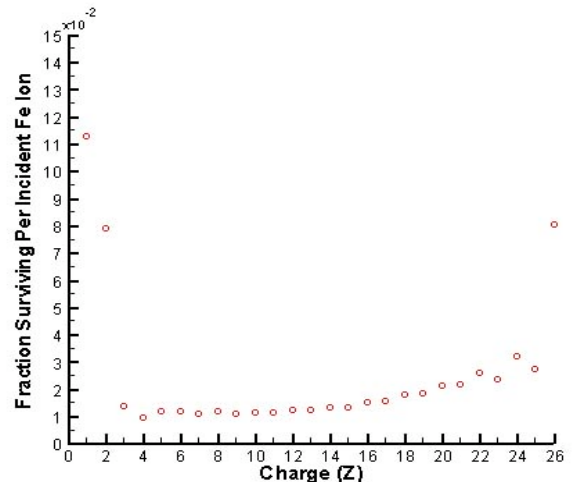


Fig. 7 Calculated fragment fluence for 1 A GeV ion beam behind 23 g/cm² of PMMA.

integral kernel of equation (26) is controlled by the forward reactive cross section $j_{k,for}(\theta, \phi, E, E')$ with its highly peaked structure given by equations (18) or (21) depending on particle type. The angular dependence of the forward peak of fragmenting Ca ions at 100 and 1,000 A MeV is shown in Fig. 6. The low-energy ions with limited range have transverse components on the order of 10 degrees reducing to a few degrees at high energies. It should be clear that the added divergence added by multiple Coulomb scattering of such fragments (Fig. 3) is negligible to the large angular widths of the fragmentation event (Fig. 6) further justifying equation (25).

Note that the low energy ions have limited range and will contribute little to the transported flux (see Fig. 1) or nuclear reactions (see Fig. 5). The higher energy ions, with their much longer pathlengths giving more important contributions, are related to only a very small angle of acceptance (few degrees) at the boundary. The form of the kernel leads directly to a Gauss-Hermite expansion and evaluation over the angle of production. Although the neutron Neumann series for the forward components converge more slowly since their contribution to the neutron flux is not limited by atomic interactions these higher energy neutrons will be adequately evaluated by similar procedures. Higher order asymptotic terms can be evaluated with similar iteration of equation (26) if required but all indications are that the first such correction will be small for space radiation. This leaves the diffuse components of neutrons and light ions produced in the collision of the forward components and transported by equation (23) to be resolved (see for example, Clowdsley et al. 2000).

The transport from the low-energy neutron and light-ion isotropic sources in equation (23) dominates the solution below about 70 A MeV (see Fig. 4). In this region light-ion transport is completely dominated by the atomic interaction terms and only a very small fraction have nuclear reactions making only minor contributions to the particle fields. This is especially true for the target fragments that can be solved in closed form (Wilson 1977, Cucinotta et al. 1991). The transport solution for the isotropic ion source terms to the lowest order perturbation is given by

$$j_{,iso}^o(\mathbf{x}, E) = \int_E^E dE' A_j P_j(E) E' \int d\Omega d\Omega' j_{k,iso,r}(\theta, \phi, E, E') \int_{k,for}(\mathbf{x} + [R_j(E) - R_j(E')] \hat{\mathbf{r}}, E) / S_j(E) P_j(E) \quad (27)$$

and will give highly accurate solutions to equation (23) since very few of the ions will have reactions (see Fig. 5), but could be easily corrected using the HZETRN light-ion propagator applied to the diffusive source terms. Note the E integral effectively sums the ion source terms along direction $\hat{\mathbf{r}}$ from the boundary to \mathbf{x} . Also, the nuclear survival terms $P_j(E)$ are all near unity (see Fig. 5 showing $1 - P_j(E)$).

THE BENCHMARK

The current status of computational procedures are detailed by Tweed et al. (2004) with validation of these procedures by Walker et al. (2004). The benchmark quantities requested are for shielding materials of polyethylene, polymethyl metachrylate (PMMA), aluminum, and lead over the thickness range of 5 to 30 g/cm². The quantities requested are:

Dose (unit fluence):

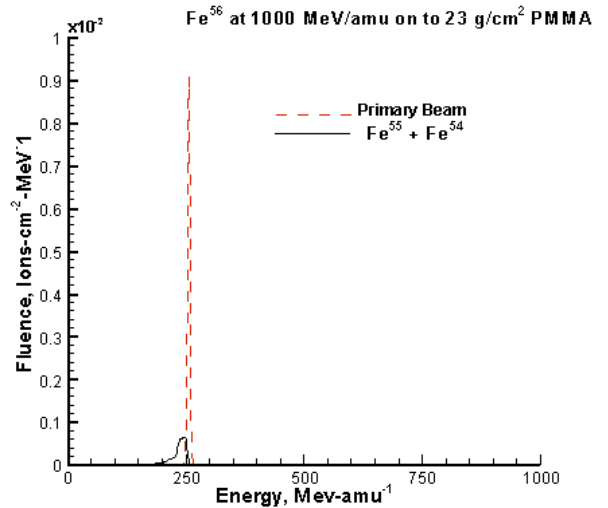


Fig. 8 Iron ion spectra after 23 g/cm² of PMMA.

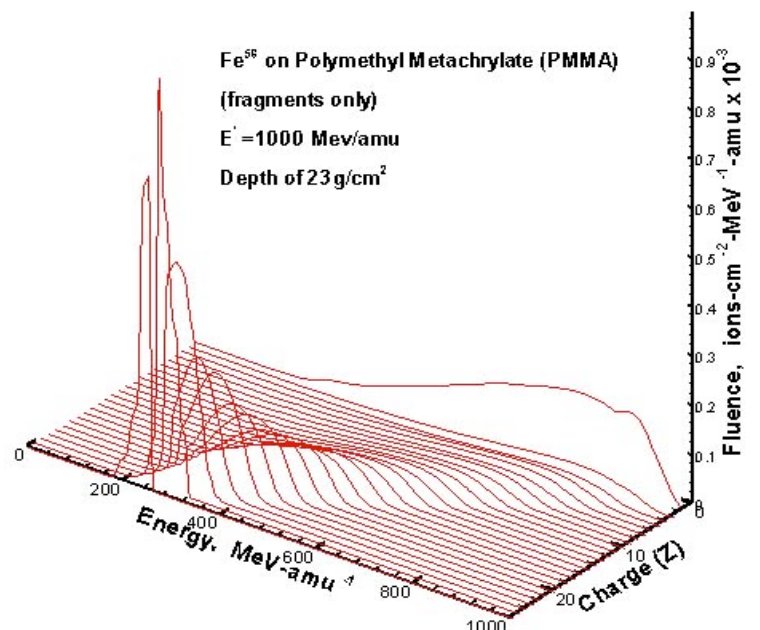


Fig. 9 Iron ion fragment spectra behind 23 g/cm² of PMMA.

$$D(x) = K \int d \int dE L_j(E) j(x, E)$$

Track averaged LET:

$$\text{LET}_{\text{trk}} = \int d \int dE L_j(E) j(x, E) / \int d \int dE j(x, E)$$

Dose averaged LET:

$$\text{LET}_{\text{dose}} = \int d \int dE L_j(E)^2 j(x, E) / \int d \int dE L_j(E) j(x, E)$$

Fraction of Fe-ions:

$$F_{\text{surviving}}(x) = \int d \int dE j(x, E) / \text{incident ion fluence (unity)}$$

Fragment spectrum at 23 g/cm² PMMA:

$$F_j(x, E) = \int d j(x, E) / \text{incident ion fluence (unity)}$$

where K is conversion from MeV/g to nGy (K=1.602). In that the full angular dependence is lacking in the present computational model (Tweed et al. 2004), we have fit a re-normalization constant to the light ion data of Zeitlin, Miller, and Heilbronn with resulting values of 0.02 (Z=1) and 0.08 (Z=2) as discussed by Walker et al. (2004). The dose, track and dose averaged LET, and fraction of surviving Fe-ions are given in Table 1. The iron ion range, R₀, for each target material is given in the table. The fragment charge spectra penetrating 23 g/cm² of PMMA is given in Fig. 7. The energy spectra of the penetrating iron ions and iron fragments are shown in Fig. 8. The shift of the iron fragment spectra to lower energies relative to the surviving beam particles resulting from loss of inertia is clearly seen in the graph. Similar observations were made in the neon beam experiments of Schimmerling et al. (Shavers et al. 1993). The ion fragment spectra are shown in Fig. 9.

CONCLUSIONS

The present benchmark is a useful exercise for comparison of computational procedures and atomic/nuclear database. The first several months of the current project has been mainly focused on advancing computational procedures (Tweed et al. 2004), validation of those procedures (Walker et al. 2004), and providing a sensitivity analysis on the 14,365 nuclear parameters required for space radiation simulations (Heinbockel et al. 2004). This has left little time for improving the physical description of the transport process that is further hampered by lack of a supporting basic nuclear physics program. The main progress is towards implementing multiple Coulomb scattering into the formalism to be followed by off axis nuclear fragmentation components with a simplified nuclear

Table 1. Benchmark parameters for 1 A GeV iron ions in the four requested materials.

Polyethylene (R ₀ = 25.3 g/cm ²)						
Depth (g/cm ²)	<LET> _{trk} (keV/ m)	<LET> _{dose} (keV/ m)	Dose (nGy)	Fraction Surviving		
				Fe ⁵⁶	Fe ^{55,54}	Total
5	112.9	142.4	180.8	0.50	0.030	0.53
10	92.3	139.2	147.9	0.25	0.032	0.29
15	82.3	143.4	131.9	0.13	0.025	0.15
20	81.1	163.8	129.9	0.067	0.019	0.085
25	98.5	274.9	157.8	0.035	0.0076	0.043
30	33.0	295.7	52.8	0	0	0
PMMA (R ₀ = 26.1 g/cm ²)						
Depth (g/cm ²)	<LET> _{trk} (keV/ m)	<LET> _{dose} (keV/ m)	Dose (nGy)	Fraction Surviving		
				Fe ⁵⁶	Fe ^{55,54}	Total
5	116.1	143.7	186.1	0.54	0.029	0.57
10	96.3	141.0	154.1	0.29	0.032	0.32
15	86.1	144.8	138.0	0.16	0.027	0.19
20	84.7	162.5	135.7	0.088	0.021	0.11
25	116.9	301.7	187.2	0.050	0.015	0.065
30	42.3	334.3	67.8	0	0	0
Aluminum (R ₀ = 33.9 g/cm ²)						
Depth (g/cm ²)	<LET> _{trk} (keV/ m)	<LET> _{dose} (keV/ m)	Dose (nGy)	Fraction Surviving		
				Fe ⁵⁶	Fe ^{55,54}	Total
5	133.3	150.1	213.5	0.78	0.0093	0.79
10	119.2	151.3	191.0	0.61	0.015	0.63
15	109.4	154.6	175.2	0.48	0.017	0.50
20	104.5	162.3	166.7	0.38	0.018	0.40
25	104.5	179.1	167.4	0.30	0.018	0.32
30	120.3	229.9	192.7	0.24	0.017	0.25
Lead (R ₀ = 50.5 g/cm ²)						
Depth (g/cm ²)	<LET> _{trk} (keV/ m)	<LET> _{dose} (keV/ m)	Dose (nGy)	Fraction Surviving		
				Fe ⁵⁶	Fe ^{55,54}	Total
5	147.2	152.0	235.8	0.93	0.0015	0.93
10	144.0	154.3	230.6	0.86	0.0028	0.87
15	141.5	157.3	226.7	0.80	0.0040	0.81
20	139.9	161.5	224.2	0.75	0.0050	0.75
25	139.9	167.3	224.1	0.69	0.0058	0.70
30	141.9	175.8	227.3	0.65	0.0065	0.65

model. The next step will be detailed studies of the first Neumann term including straggling and multiple Coulomb scattering to better relate to geometries found in the laboratory setting.

REFERENCES

- Armstrong, T.W., Colburn, B.L. Predictions of secondary neutrons and their importance to radiation effects inside the international space station. *Radiat. Meas.* 33: 229-234; 2001.
- Cloudsley, M.S., et al. A comparison of the multigroup and collocation methods for solving the low-energy neutron Boltzmann equation. *Can. J. Phys.* 78: 45-56; 2000.
- Cucinotta, F. A., and R. R. Dubey, Alpha-Cluster Description of Excitation Energies in ^{12}C (^{12}C , 3) X at 2.1A GeV, *Phys. Rev.*, **C50**, pp. 979-984; 1994.
- Cucinotta, F. A.; Katz, R.; Wilson, J. W.; Townsend, L. W.; Shinn, J. L.; and Hajnal, F. Biological Effectiveness of High-Energy Protons: Target Fragmentation. *Radiation Research* 127:130-137; 1991.
- Cucinotta, F. A.; Wilson, J. W.; Shinn, J. L.; and Tripathi, R. K: Assessment and Requirements of Nuclear Reaction Data Bases for GCR Transport in the Atmosphere and Structures, *Adv. Space Res.*, 21(12): 1753-1762 1998
- Leakeas, C.L., Larsen, E.W., Generalized Fokker-Planck approximation of particle transport with highly forward-peaked scattering. *Nucl. Sci. Eng.* 137: 236-250; 2001.
- Pinsky, L., Carminati, F., Ferrari, A. Simulation of space Shuttle neutron measurements with FLUKA. *Radiat. Meas.* 33: 335-339; 2001.
- Pomraning, G.C., The screened Rutherford pencil beam problem with heterogeneities. *Nucl. Sci. Eng.* 136; 1-14; 2000.
- Prinja, A.K., Pomraning, G.C., A generalized Fokker-Planck model for transport of collimated beams. *Nucl. Sci. Eng.* 137: 227-235; 2001.
- Ranft, J. The FLUKA and KASPRO Hadronic Cascade Codes. *Computer Techniques in Radiation Transport and Dosimetry*, W. R. Nelson and T.M. Jenkins, eds, Plenum Press, pp. 339-371, 1980
- Schimmerling, W., Rapkin, M., Wong, M., Howard, J. The propagation of relativistic heavy ions in multielement beam lines. *Medical Phys.* 13: 217-228; 1986.
- Shavers, M. R., Curtis, S.B., Miller, J., Schimmerling, W. The fragmentation of 670A MeV Neon-20 as a function of depth in water. II. One-generation transport theory. *Radiat. Res.* 124: 117-130; 1990.
- Shavers, M. R., Frankel, K., Miller, J., Schimmerling, W., Townsend, L. W., Wilson, J. W., The Fragmentation of 670 A MeV Neon-20 as a Function of Depth in Water. III. Analytic Multigeneration Transport Theory. *Radiat. Res.*, 134(1): 1-14; 1993.
- Shinn, J.L., Cucinotta, F.A., Simonsen, L.C., Wilson, J.W., Badavi, F.F., Badhwar, G.D., Miller, J., Zeitlin, C., Heilbronn, L., Tripathi, R.K., Cloudsley, M.S., Heinbockel, J.H., Xapsos, M.A. "Validation of a Comprehensive Space Radiation Transport Code", *IEEE Transactions on Nuclear Science*, 45: 2711-2719; 1998.
- Tripathi, R.K., Townsend, L.W., Kahn, F. Role of intrinsic width in fragment momentum distributions in heavy ion collisions, *Phys. Rev. C*, 48(4), R1775-R1777; 1994.
- Tweed, J., Walker, S.A., Wilson, J.W., Cucinotta, F.A., Tripathi, R.K., Blattnig, S., Mertens, C.J. Computational Methods for the HZETRN Code. 35th COSPAR, Paris France 18-25, July 2004.
- Walker, S.A., Tweed, J., Wilson, J.W., Cucinotta, F.A., Tripathi, R.K., Blattnig, S., Zeitlin, C., Heilbronn, L., Miller, J. Validation of the HZETRN Code for Laboratory Exposures with 1 A GeV Iron Ions in Several Targets. 35th COSPAR, Paris France 18-25, July 2004.
- Wilson, J.W., Khandelwal, G.S. Proton dose approximation in convex geometry. *Nucl. Tech.* 23: 298-305;1974.
- Wilson, J.W. *Analysis of the theory of high-energy ion transport*. NASA TN D-8381, 1977.
- Wilson, J.W., Townsend, L.W., Bidasaria, H.B., Schimmerling, W., Wong, M. Howard, J. 20-Ne depth-dose relations in water. *Health Phys.* 46: 1101-1111; 1984.
- Wilson, J. W., Badavi, F. F., Methods of Galactic Heavy Ion Transport. *Radia. Res.* 108: 231; 1986.
- Wilson, J. W.; Townsend, L. W.; and Badavi, F. F.: A Semiempirical Nuclear Fragmentation Model. *Nucl. Inst. & Methods* B18: 225; 1987a.
- Wilson, J. W.; Townsend, L. W.; and Badavi, F. F.: Galactic Cosmic Ray Propagation in Earth's Atmosphere. *Radiat. Res.* 109: 173-183; 1987b.
- Wilson, J.W. S. Y. Chun, W. W. Buck, and L. W. Townsend: High Energy Nucleon Data Bases. *Health Phys.*, 55: 817-819; 1988.

- Wilson, J. W., Townsend, L. W., Schimmerling, W., Khandelwal, G. S., Khan, F., Nealy, J. E., Cucinotta, F. A., Simonsen, L. C., Shinn, J. L., Norbury, J. W. *Transport Methods and Interactions for Space Radiations*. NASA RP-1257, 1991.
- Wilson, J. W., Shavers, M. R., Badavi, F. F., Miller, J., Shinn, J. L., and Costen, R. C., Nonperturbative Methods in HZE Propagation. *Radiat. Res.* 140: 241-244; 1994a.
- Wilson, J. W., Townsend, L. W., Shinn, J. L., Badavi, F. F., Lamkin, S. L., Galactic Cosmic Ray Transport Methods: Past, Present, and Future. *Adv. Space Res.* 14: (10) 841 - (10) 852, 1994b.
- Wilson, J. W., R. K. Tripathi, F. A. Cucinotta, J. L. Shinn, F. F. Badavi, S. Y. Chun, J. W. Norbury, C. J. Zeitlin, L. H. Hielbronn, and J. Miller, NUCFRG2, *An Evaluation of the Semiempirical Nuclear Fragmentation Database*, NASA TP-3533, 1995.
- Wilson, J. W., Cucinotta, F. A., Tai, H., Shinn, J. L., Chun, S. Y., Tripathi, R.K., Sihver, L. (1998) Transport of light ions in matter. *Adv. Space Res.* 21(12): 1763-1771
- Wilson, J.W., Tweed, J., Tai, H., and Tripathi, R.K. A simple model for straggling evaluation. *Nucl Inst & Methods B* 194: 389-392; 2002.
- Wilson, J.W., Tripathi, R.K., Qualls, G.D., Cucinotta, F.A., Prael, R.E., Norbury, J.W., Heinbockel, J.H., and Tweed, J. Space Radiation Transport Methods Development, *Adv. Space Res.* In press.
- Wong, M., Schimmerling, W., Phillips, H., Ludewigt, B.A., Landis, D., Walton, J., Curtis, S.B. The multiple coulomb scattering of very heavy charged particles. *Medical Phys.* 17(2):163-171; 1989.
- Zeitlin, C., Heilbronn, L., Miller, J., Rademacher, S.E., Borak, T., Carter, T.R., Frankel, K.A., Schimmerling, W., Stronach, C.E. Heavy fragment production cross sections from 1.05 GeV/nucleon ⁵⁶Fe in C, Al, Cu, Pb, and CH₂ targets. *Phys. Rev. C* 56: 388-397; 1997.